Mismatched alloy nanowires for electronic structure tuning

Joanne W. L. Yim,[1,2] Costas P. Grigoropoulos,[3,4] and Junqiao Wu[1,2,a]

[1]Department of Materials Science and Engineering, University of California, Berkeley, California 94720, USA
[2]Materials Sciences Division, Lawrence Berkeley National Laboratory, Berkeley, California 94720, USA
[3]Department of Mechanical Engineering, University of California, Berkeley, California 94720, USA
[4]Environmental Energy Technologies Division, Lawrence Berkeley National Laboratory, Berkeley, California 94720, USA

Electronic structure engineering is essential for producing materials suited for efficient solid-state devices. Mismatched semiconductors offer wide tunability of electronic structure with only a small change in composition. Here, we report a combined compound-elemental source vapor transport method for synthesis of mismatched alloy nanowires (NWs) of $ZnSe_{1-x}Te_x$ across the composition range. The alloy composition can be continuously tuned by varying the growth temperature from ZnSe ($x = 0$) at higher temperature to ZnTe ($x = 1$) at lower temperature. The nanowires have structure and bandgaps consistent with their compositions, with lattice parameters varying with Vegard's law and emissions following predicted extreme bandgap bowing. © 2011 American Institute of Physics. [doi:10.1063/1.3666223]

Semiconductor nanowires (NWs) have received much attention recently for their potential as building blocks for future electronics, optoelectronics, and energy-conversion devices. Tuning the electronic structure, including the bandgap, band offset, carrier effective mass, and density of states, of the material by composition control is of extreme importance to match the material to the application. Much progress has been made to synthesize tunable NWs of group IV alloys,[1] III-V alloys,[2] and II-VI alloys.[3,4] However, the majority are cation substitutions, with the few anion substitutions reported[4] consisting entirely of Se-S alloys. This is mostly because the Se-S anion pair, similar to many isoelectronic cation pairs, is well-matched in size and electronegativity; thus, the material readily accepts substitutions from a thermodynamic point of view. In contrast, mismatched alloys are more difficult to synthesize, reaching only 17% As in the prototypical mismatched alloy system $GaAs_xN_{1-x}$, even using a highly non-equilibrium molecular beam epitaxy (MBE) growth technique.[5] However, even small mismatched substitutions are capable of producing significant electronic structure changes, resulting in abnormal bandgap bowing and, more uniquely, density of states engineering.[6] Mismatched alloys have been used to create intermediate-band solar cells[7] and the density of states shape tuning is predicted to enhance the Seebeck coefficient for improved thermoelectric efficiency.[8]

In this paper, we present a combined compound-elemental source vapor transport method and have grown alloy NWs of a non-trivial mismatch, ZnSeTe, across the composition range.

Group VI elements have electronegativities ranging from 2.08 to 3.47 (from Te up to O) using the Pauling scale.[9] At one extreme, S and Se are very similar, with only a 0.1 difference in electronegativity, and on the other, Te and O differ by 1.39. Se and Te have a moderate electronegativity difference, at 0.3, and both ZnSe and ZnTe are predominantly stable in the zincblende structure, with the ZnTe lattice parameter 7% larger. The moderate mismatch in anions makes zinc selenotelluride an ideal candidate for developing growth techniques for mismatched alloys, although synthesizing ZnSeTe is not without challenges. Historically, bulk ZnSeTe have been grown by physical vapor transport[10] or by heating powders of ZnSe and ZnTe together at high temperatures.[11] Thin films by evaporation displayed evidence of ZnSe-rich regions through Raman spectroscopy.[12] Lower-temperature methods produced thin films with reasonable crystal quality by metalorganic vapor phase epitaxy (MOVPE) on InP substrates[13] and fully-relaxed films on GaAs substrates by metalorganic chemical vapor deposition (MOCVD).[14] Previous works on selenium/tellurium NWs alloys have yielded only limited compositions and architectures. Dong et al. synthesized small segments of ZnSeTe in transition regions between ZnSe and ZnTe ends of quantum rods by a solution-liquid-solid method, producing structures that exhibited broad absorption features indicative of ZnSe and ZnTe with a sloping region in between.[15] Only one other composition, $ZnSe_{0.95}Te_{0.05}$ nanotips, has been grown.[16]

The combined compound-elemental source vapor transport growth was carried out in a 1 in. diameter silica half-shell hinged tube furnace (Lindberg Blue/M TF55035). The tube furnace has a single heating zone, referred to here as T_{max}, which corresponds to a flat temperature zone at the center 12 cm of the furnace, and from there the temperature drops off symmetrically toward the outer ends. A mechanical rotary pump is used to evacuate the chamber to 1×10^{-2} torr before beginning the growth run. The NWs were grown on 100 nm/500 μm thermally grown SiO_2/Si wafers cut into 1×1 cm sq. Prior to preparation with a catalyst layer, the wafers were sequentially sonicated in acetone, isopropanol, and deionized (DI) water, then dried with compressed air. Either Au colloids or a Pd/Au thin film catalysts were used, following the procedure of Nicu et al. or Chung et al.[17] The source powders were loaded into either a silica or an alumina

a)Author to whom correspondence should be addressed. Electronic mail: wuj@berkeley.edu.

boat and the boat was placed in the chamber. Two source materials at different temperatures were used: an elemental source (Te) at lower temperature T_L and a compound source (ZnSe) at T_{max} downstream.[18] Substrates were placed flat into a half-shell silica tube and positioned downstream of the source boats at temperature T_{subs}. The chamber was evacuated and flushed with ultra high-purity argon in alternating pump and purge cycles to remove residual oxygen. The furnace was ramped to the "set temperature" at 50–60 °C/min and held there for 15–60 min. After the heating elements were de-energized, the furnace was allowed to cool naturally down to ~350 °C, and then more aggressively by opening the furnace hinge until the chamber cooled to below 100 °C. The inert gas flow and vacuum pump remained on while the chamber cooled. The growth conditions for the ZnSeTe alloy are as follows: $T_{max} = 800$ °C, $T_L = 420$–540 °C, $T_{subs} = 560$–700 °C, $k_f = 100$ sccm Ar, $P = 10$ torr, $t = 30$ min, 25 mg ZnSe, and 500 mg Te. NWs of each pure composition, ZnSe and ZnTe, were synthesized under the same conditions with the appropriate compound source, without the additional elemental source.

The compositions of the NWs can be roughly identified visually macroscopically, since ZnSe NWs are yellow and ZnTe NWs are red-orange. In the growth region, from high T_{subs} to low T_{subs}, the resultant products are ZnSe-like to ZnTe-like. Regions without catalysts did not have NW products.

The nanostructures grew in a disorganized fashion, with some structures lying nearly flat on the substrate and others growing straight up (Fig. 1, top). A wide variety of 1-D nanostructure sizes and shapes were attained. Many were tapered and had rough sidewalls.[18] The bases of the tapered structures can be quite large, but they decrease in diameter into the 10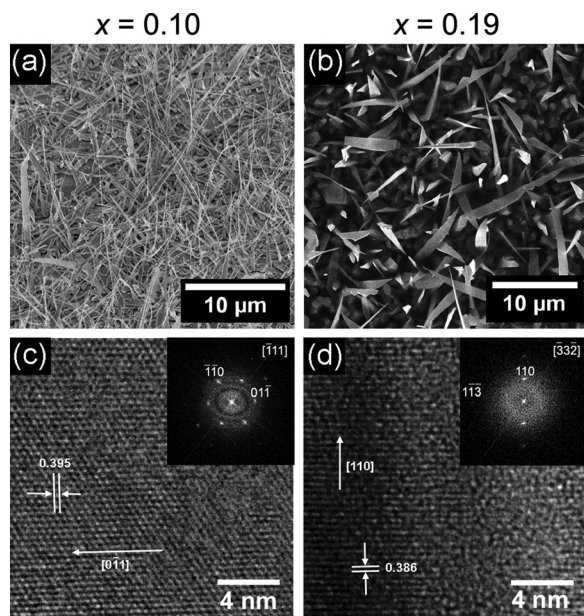0-nm range. Round Au-rich balls can be found at the tips of some nanostructures, confirming vapor-liquid-solid-driven axial growth. The difference between the catalyst size and the nanostructure's diameter suggests either extensive sidewall growth or catalyst depletion as the structure formed. The roughness of the sidewalls argues that the former is the most likely culprit here.

Using energy dispersive x-ray spectroscopy (EDX), we determined that the composition does not vary significantly along the length of the structure.[18] Due to the preferential incorporation of Se,[14] in spite of Te being supplied in excess, a greater number of compositions on the Se-rich side were attained. Given the lack of preferential alignment in the as-grown structures, the x-ray diffraction (XRD) shows that the NWs are zincblende across the composition range (Fig. 2). The diffraction spectra shift from the ZnTe zincblende pattern (JC-PDS 15-0476) to the ZnSe (JC-PDS 37-1463). Plotted against the EDX-determined Te content, the lattice parameter shows a clear linear trend, consistent with Vegard's law. Small peaks from the hexagonal polytype (JCPDS 80-0008) can be seen in the ZnSe pattern and even the low Te content specimens. Higher Te content eliminates this tendency, since ZnTe rarely assumes the hexagonal structure. At intermediate compositions, the XRD signal drops considerably with respect to the endpoint signal strength. This is primarily due to reduced specimen availability; the growth efficacy drops away from the composition endpoints, so there are fewer structures to contribute in the middle compositions.

Transmission electron microscopy (TEM) was used to investigate the quality of the nanostructures. Despite the non-uniformity of the outer appearance, the nanostructures were still highly crystalline (Fig. 1, bottom). The nanowires were indexed to zincblende, with the appearance of
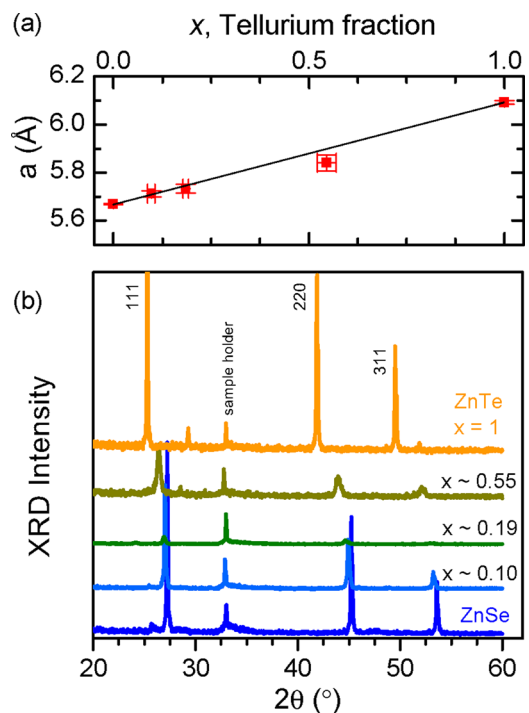

FIG. 1. SEM images of $ZnSe_{1-x}Te_x$ nanowires with (a) $x = 0.10$ and (b) $x = 0.19$. The wires had no preferred registration to the growth substrate. High-resolution TEM images and the corresponding FFTs (inset) of the nanowires with (c) $x = 0.10$ and (d) $x = 0.19$. The orientation of the long axis is indicated by the arrow and the corresponding lattice spacing is given in nanometers. Micrographs for $x = 0.55$ can be found in the supplementary material.[18]

FIG. 2. (Color online) XRD from as-grown $ZnSe_{1-x}Te_x$ nanowires. (a) Zinc-blende lattice parameter, a (Å), determined from XRD, graphed as a function of Te fraction, x, as measured by EDX. (b) XRD spectra in decreasing Te fraction, ZnTe to ZnSe, from top to bottom. The zincblende peaks shift linearly to larger angles for decreasing Te content, following Vegard's law.
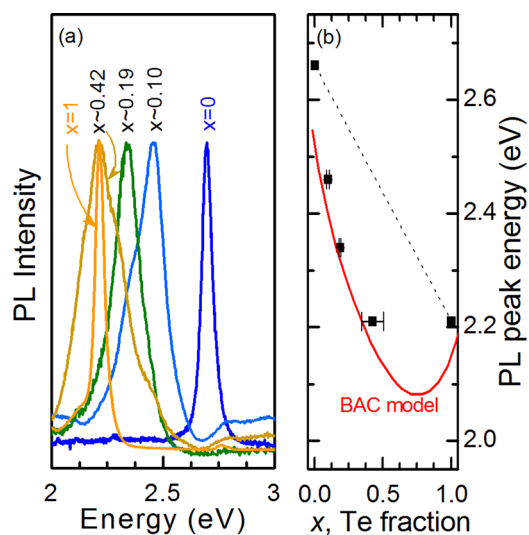
FIG. 3. (Color online) (left) Photoluminescence response from as-grown ZnSe$_{1-x}$Te$_x$ nanowires, taken at room-temperature. (right) Near-band-edge peak energy plotted as a function of Te fraction, x. The bandgap bowing as predicted by the BAC model is shown[20] (solid curve), which contrasts with the linear interpolation in well-matched alloys (dotted line).

forbidden reflections possibly due to the chemical disorder of replacing some Se with Te. The well-mixed crystallinity was also observed through the appearance of one-mode Raman behavior.[18]

Photoluminescence measurements were also taken. The change in bandgap energy in mismatched alloys has been well-described by the band anti-crossing (BAC) model.[6] The BAC model describes the electronic structure of the alloy as a hybridization of the band states of the majority constituent with the localized states of the minority constituent, leading to extreme band bowing and intermediate band formation. For ZnSeTe, both valence and conduction BAC are necessary to explain the evolution of the band structure across the entire composition range.[19] In well-matched alloys such as S-Se alloys, the bandgap of the alloy follows a linear interpolation of the two end-point materials; in the mismatched ZnSeTe, in contrast, the BAC results in an extreme bandgap bowing. Indeed, our NWs display photoluminscence corresponding to a shift in bandgap consistent with the strong bowing in ZnSeTe bulk samples, obeying the valence BAC for compositions closer to ZnSe and conduction BAC closer to ZnTe (Fig. 3). None of the middle compositions displayed the red emission that was observed in some pure ZnTe nanowires samples.

In summary, using a dual compound-elemental source method, we have synthesized NWs of the mismatched alloy, ZnSeTe, with optical and structural properties of the NWs sensitively determined by their compositions. NWs of a particular desired composition can be obtained by controlling the substrate temperature. The extraordinary band engineering potential in mismatched alloys has advantages for photovoltaic, thermoelectric, and optoelectronic applications.

[1] J. E. Yang, C. B. Jin, C. J. Kim, and M. H. Jo, Nano Lett. **6**(12), 2679 (2006).
[2] C. S. Jung, H. S. Kim, G. B. Jung, K. J. Gong, Y. J. Cho, S. Y. Jang, C. H. Kim, C.-W. Lee, and J. Park, J. Phys. Chem. C **115**(16), 7843 (2011); Z. H. Wu, M. Sun, X. Y. Mei, and H. E. Ruda, Appl. Phys. Lett. **85**(4), 657 (2004); T. Kuykendall, P. Ulrich, S. Aloni, and P. Yang, Nature Mater. **6**(12), 951 (2007).
[3] F. Gu, Z. Yang, H. Yu, J. Xu, P. Wang, L. Tong, and A. Pan, J. Am. Chem. Soc. **133**(7), 2037 (2011); Y.-F. Lin, Y.-J. Hsu, S.-Y. Lu, K.-T. Chen, and T.-Y. Tseng, J. Phys. Chem. C **111**(36), 13418 (2007); R. Venugopal, P.-I. Lin, and Y.-T. Chen, J. Phys. Chem. B **110**(24), 11691 (2006); L. W. Yin and S. T. Lee, Nano Lett. **9**(3), 957 (2009).
[4] A. Pan, H. Yang, R. Liu, R. Yu, B. Zou, and Z. Wang, J. Am. Chem. Soc. **127**(45), 15692 (2005); M. Wang, G. T. Fei, Y. G. Zhang, M. G. Kong, and L. D. Zhang, Adv. Mater. **19**(24), 4491 (2007); Y. Liang, H. Y. Xu, and S. Hark, Cryst. Growth Des. **10**(10), 4206 (2010).
[5] K. M. Yu, S. V. Novikov, R. Broesler, I. N. Demchenko, J. D. Denlinger, Z. Liliental-Weber, F. Luckert, R. W. Martin, W. Walukiewicz, and C. T. Foxon, J. Appl. Phys. **106**(10), 103709 (2009).
[6] W. Shan, W. Walukiewicz, J. W. Ager, E. E. Haller, J. F. Geisz, D. J. Friedman, J. M. Olson, and S. R. Kurtz, Phys. Rev. Lett. **82**(6), 1221 (1999); W. Walukiewicz, W. Shan, K. M. Yu, J. W. Ager, E. E. Haller, I. Miotkowski, M. J. Seong, H. Alawadhi, and A. K. Ramdas, Phys. Rev. Lett. **85**(7), 1552 (2000).
[7] N. López, L. A. Reichertz, K. M. Yu, K. Campman, and W. Walukiewicz, Phys. Rev. Lett. **106**(2), 028701 (2011); K. M. Yu, W. Walukiewicz, J. Wu, W. Shan, J. W. Beeman, M. A. Scarpulla, O. D. Dubon, and P. Becla, Phys. Rev. Lett. **91**(24), 246403 (2003).
[8] J.-H. Lee, J. Wu, and J. C. Grossman, Phys. Rev. Lett. **104**(1), 016602 (2010).
[9] W. Gordy, Phys. Rev. **69**(11–12), 604 (1946).
[10] Y. V. Korostelin, V. I. Kozlovsky, A. S. Nasibov, and P. V. Shapkin, J. Cryst. Growth **159**(1–4), 181 (1996).
[11] V. Valdna, J. Hiie, U. Kallavus, A. Mere, and T. Piibe, J. Cryst. Growth **161**(1–4), 177 (1996).
[12] A. J. Pal and J. Mandal, J. Alloys Compd. **216**(2), 265 (1995).
[13] M. Strassburg, M. Strassburg, O. Schulz, U. W. Pohl, A. Hoffmann, D. Bimberg, A. G. Kontos, and Y. S. Raptis, J. Cryst. Growth **248**, 50 (2003).
[14] A. Kamata, H. Yoshida, S. Chichibu, and H. Nakanishi, J. Cryst. Growth **170**(1–4), 518 (1997).
[15] A. Dong, F. Wang, T. L. Daulton, and W. E. Buhro, Nano Lett. **7**(5), 1308 (2007).
[16] S. J. Chang, C. H. Hsiao, S. C. Hung, S. H. Chih, B. W. Lan, S. B. Wang, S. P. Chang, Y. C. Cheng, T. C. Li, and B. R. Huang, J. Electrochem. Soc. **157**(1), K1 (2010).
[17] H.-S. Chung, Y. Jung, T. J. Zimmerman, S.-H. Lee, J. W. Kim, S. H. Lee, S. C. Kim, K. H. Oh, and R. Agarwal, Nano Lett. **8**(5), 1328 (2008); L. Nicu, M. Guirardel, F. Chambosse, P. Rougerie, S. Hinh, E. Trevisiol, J.-M. Francois, J.-P. Majoral, A.-M. Caminade, E. Cattan et al., Sens. Actuators B **110**(1), 125 (2005).
[18] See supplementary material at http://dx.doi.org/10.1063/1.3666223 for experimental setup schematic, SEM and TEM of another composition, TEM/EDX of a single nanostructure, and Raman spectroscopy results.
[19] J. Wu, W. Walukiewicz, K. M. Yu, J. W. Ager, E. E. Haller, I. Miotkowski, A. K. Ramdas, C.-H. Su, I. K. Sou, R. C. C. Perera et al., Phys. Rev. B **67**(3), 035207 (2003).
[20] J. Wu, W. Walukiewicz, K. M. Yu, W. Shan, J. W. Ager, E. E. Haller, I. Miotkowski, A. K. Ramdas, and C.-H. Su, Phys. Rev. B **68**(3), 033206 (2003).